## PAPER

Check for updates

# Synthesis of an imine-type nickel complex and investigation of its electrocatalytic activity for H₂ evolution†

Lan H. Le, [ID] Ngoc H. Pham, Phong D. Tran [ID] and Tung H. To [ID] *

We report on the synthesis and characterization of an imine-type nickel complex produced *via* the complexation of an *in situ* generated 2-(iminomethyl)phenol ligand with Ni[II] ion. The use of this complex as an electrocatalyst for H₂ evolution in a DMF solution, with acetic acid as the proton source, was investigated in detail, employing both experimental analyses (electrochemical analysis, spectroscopy analysis) and theoretical analysis (plateau current analysis). The overpotential required for H₂ evolution is about 590 mV with a faradaic efficiency of 49% after 3 hours bulk electrolysis, competing with the two-electron reduction of free-imine groups in the ligand. The maximal TOF was estimated to be about 12 860 $s^{-1}$ on the basis of a CECE mechanism.

## Introduction

In the 21st century, the search for alternative energies to replace traditional fossil fuels is gaining great attention from scientists, energy companies, and countries around the world. Among the potential candidates, hydrogen (H₂) is identified as a clean, renewable energy source and could become a key energy carrier in the future economy.[1,2] However, the production of hydrogen on a large scale still faces significant challenges.[2,3] From a technical point of view, the production of green H₂ from water electrolysis faces difficulties because of slow kinetics; thus, the identification of viable catalysts is highly demanded.[4] Catalysts made of noble metals such as Pt and IrO₂ are excellent in terms of catalytic performance, but their rarity likely limits their use in industrial H₂ production. Hence, an ongoing active research direction has focused on identifying alternative catalysts that can be produced using earth-abundant elements.[5–11] Inspired by the natural hydrogenases,[12] which efficiently catalyses the reduction of protons into hydrogen, numerous studies have focused on designing molecular catalysts using first-row transition metals (Fe, Co, and Ni) for catalytic H₂ evolution.[13–16] Among the nickel-based molecular catalysts that have been reported, we can mention several promising candidates such as nickel–polyaza macrocyclic complexes;[17] nickel–polypyridine complexes,[16,17] nickel–phosphine complexes[17] or nickel–thiolate complexes.[17] Although the salen compound, *N,N'*-ethylenebis(salicylimine), is one of the well-known ligands in the coordination chemistry, nickel–salen complexes have not been studied intensively as

catalysts for the H₂ evolution reaction.[18–23] One reason for the lack of interest in salen-type ligands may be the difficulty in tuning their structure. For instance, it is possible to (i) add functional groups (electron withdrawing or electron donating groups); (ii) use phosphorus or sulfur as the donating groups instead of oxygen in the traditional salen ligands (N₂O₂), or (iii) change the length of the conventional 2-carbon bridging linkage in the salen structure. In 2016, Zhan *et al.* reported on the synthesis of a nickel–diiminodiphosphine complex that catalysed H₂ evolution with moderate turnover frequencies (TOF) of 204 and 1327 per hour in acetonitrile and in an aqueous electrolyte of pH 7, respectively.[22] Robert *et al.* reported on a nickel complex with an N₂P salen ligand showing a faradaic efficiency (FE) of 85%, calculated based on 4 hours bulk electrolysis in the presence of HClO₄ acid.[18] Regarding the ligand with sulfur donors, to the best of our knowledge, no report about this modification is available, perhaps due to the difficulties in the synthesis of these ligands. Sulfur groups are considered as the soft nucleophilic reagents in the condensation reaction generating salen compounds, and they always tend to conduct the cyclization instead of remaining as free donors such as oxygen or phosphorus groups.[24,25]

Regarding the linkage alteration, the length of the bridging ligand has been mainly kept with the traditional 2-carbon linkage. An alternation of this bridging ligand length was not popular. In 2020, Liu *et al.* described a nickel complex with a five-coordinate N₃O₂ salen ligand containing a 3-carbon linkage.[21] However, the amended ligand did not offer an impressive H₂ evolution catalytic activity. Actually, an FE value of 67% was achieved after 5 hours bulk electrolysis at −1.60 V *vs.* Fc[+/0] (with an overpotential of 340 mV).

Recently, we reported the synthesis of cobalt dinuclear complexes using a "short" salen ligand containing a 1-carbon linkage. These complexes showed attractive H₂ evolution

University of Science and Technology of Hanoi, Vietnam Academy of Science and Technology, 18 Hoang Quoc Viet, Hanoi, Vietnam. E-mail: to-hai.tung@usth.edu.vn

† Electronic supplementary information (ESI) available. See DOI: https://doi.org/10.1039/d4ra08116a

activity in DMF solution employing acetic acid as the proton resource; an overpotential of 470 mV was required and FE of 85–95% was obtained after 5 hours bulk electrolysis.[26] Herein, we report the synthesis, structural characterization and investigation of the catalytic $H_2$ evolution activity of a nickel complex with a "short" salen ligand.

## Experimental

All reagents and solvents were purchased from commercial sources and used without any additional purification. All reactions were performed in oven-dried glassware. $^1H$ and $^{13}C$-NMR spectra were recorded in a deuterated solvent (dimethyl sulfoxide DMSO-$d_6$) on Bruker Avance Neo 600 spectrometers (600 and 150 MHz, respectively). Chemical shifts are reported in parts per million (ppm) from tetramethylsilane (TMS) with the solvent resonance as an internal standard. Splitting patterns are designated as "s, d, t, q, and m" to indicate "singlet, doublet, triplet and multiplet", respectively. UV-vis spectra were recorded on an Agilent Cary 3500 compact instrument using a 1 cm quartz cuvette. Samples were prepared in the DMF solution. Raman spectra were recorded on a HORIBA LabRAM HR Evolution Raman Microscope in the region from 100 to 3000 cm$^{-1}$, using a 532 nm diode laser with a 0.1% filter. Fourier-transform infrared spectroscopy measurements were conducted on a Thermo Scientific Nicolet iS50 spectrometer in the region from 525 to 4000 cm$^{-1}$ using the Attenuated Total Reflection (ATR) mode. Powder samples were used for the Raman and IR measurements. Elemental analysis was carried out using the Flash 2000 (ThermoFisher) equipment. ICP-MS was measured using the Thermo Scientific iCAP RQ, and calibration curves were established for the concentration range relevant to the samples.

The pre-ligand $N,N'$-bis(salicylidene)-phenylmethanediamine (**M**) was prepared following the procedure described in our previous study.[26]

### Synthesis of [NiL]

10 mL ethanolic solution of NiCl$_2$·6H$_2$O (1.44 g; 6.06 mmol; 1.0 eq. mol) was added dropwise into 15 mL of suspension in ethanol containing the pre-ligand **M** (2.0 g; 6.06 mmol; 1.0 eq. mol) and triethylamine (6 mL). The orange precipitate appeared after 30 minutes and the reaction mixture was stirred continuously at the ambient temperature for 7 hours. The product was filtered and washed with ethanol, diethyl ether and acetone : dichloromethane mixture (1 : 1/v/v), and then dried *in vacuo* to obtain the orange powder (1.44 g; 77%).

$^1$**H-NMR** (600 MHz, DMSO-$d_6$) $\delta$ 8.56 (s, 2H, –**NH**); 7.76 (d, $J$ = 11.7 Hz, 2H, –**CH**=NH); 7.32 (dd, $J$ = 7.8, 1.9 Hz, 2H, H$_{ar}$); 7.14 (ddd, $J$ = 8.6, 6.9, 1.8 Hz, 2H, H$_{ar}$); 6.66 (d, $J$ = 8.5 Hz, 2H, H$_{ar}$); 6.54–6.48 (m, 2H, H$_{ar}$).

$^{13}$**C-NMR** (151 MHz, DMSO-$d_6$) $\delta$ 164.53; 162.86; 133.39; 133.27; 120.59; 120.20; 114.41.

**Elemental analysis.** Calculated C$_{14}$H$_{12}$N$_2$O$_2$Ni: C 56.25, H 4.05, N 9.37; found C 55.87, H 4.11, N 8.88 (%)

**ICP-MS.** Calculated C$_{14}$H$_{12}$N$_2$O$_2$Ni: Ni 19.63; found 20.00 (%)

**Electrochemistry.** Cyclic voltammograms were recorded using an AutoLab potentiostat and a conventional three-electrode setup consisting of a glassy carbon working electrode (working surface area = 0.071 cm$^2$), a platinum wire counter electrode and an Ag/AgCl (KCl 3 M) reference electrode. Ferrocene was used as an internal standard with $E^o(Fc^{+/0})$ = 0.53 V *vs.* Ag/AgCl. All studies were performed in deoxygenated DMF containing 0.1 M tetrabutylammonium tetrafluoroborate (TBATFB) as the supporting electrolyte.

Controlled-potential electrolysis (CPE) in organic media was conducted using an air-tight glass double compartment cell wherein two compartments were separated by a frit. The working compartment was fitted with a graphite electrode (working surface area = 2.0 cm$^2$) and an Ag/AgCl reference electrode. The auxiliary compartment was fitted with a Pt counter electrode. Bulk electrolysis solutions were purged with N$_2$ gas for 1 hour to eliminate the dissolved O$_2$.

H$_2$ production was quantified by gas chromatography. The gaseous product was manually sampled and analysed using a PerkinElmer Clarus 690 gas chromatographer. The analysis setup represented a 5 min method with 100 °C injection, nitrogen gas flow was 12 mL min$^{-1}$, Restek ShinCarbon ST Micropacked GC Column and Thermal Conductivity Detector (TCD) was set at 200 °C and −40 mA current.

## Results and discussion

### Synthesis and characterization of NiL complex

The nickel complex (**NiL**) was prepared *via* a one-step reaction consisting of equimolar amounts of nickel(ii) chloride and pre-ligand (**M**) in the presence of triethylamine. The reaction was kept overnight, the reaction completion was monitored by TLC. The crude compound was obtained in the form of an orange powder, which was then collected by filtration, washed intensively with ethanol, diethyl ether and an acetone–dichloromethane mixture to obtain the pure orange complex (**NiL**) (Scheme 1). The formation of the product was confirmed by physical spectroscopic analyses. In the $^1$H-NMR spectrum, the decomposition of pre-ligand (**M**) could be observed obviously throughout the lack of aromatic proton signals when the –CHC$_6$H$_5$ group at the salen-ligand bridge was removed (Fig. S1a†). The –NH protons of the imine group showed broad singlet peaks at 8.56 ppm whereas –CH– protons showed peaks at 7.77 ppm appearing in the doublet multiplicity. With the coupling constant $J$ = 12.0 Hz, we could also determine the configuration of the –CH=NH group, which is in the *cis* form. In the $^{13}$C-NMR spectrum, the resonance signals of imine carbon atoms were still at 164.5 ppm. However, there was a slight shift from 160.0 ppm to nearly 162.8 ppm for the carbon atoms in the aromatic ring, which were bonded to the oxygen atoms. This change was attributed to the influence of the Ni metal center, which reduced the electron density around the carbon atom, causing the resonance signal shift to the down-field region. Besides that, the signal of N–C–N bridging carbon initially found at 89.5 ppm in the free pre-ligand, disappeared in the **NiL** complex together with the absence of 6 other aromatic carbon signals. These observations further confirmed the
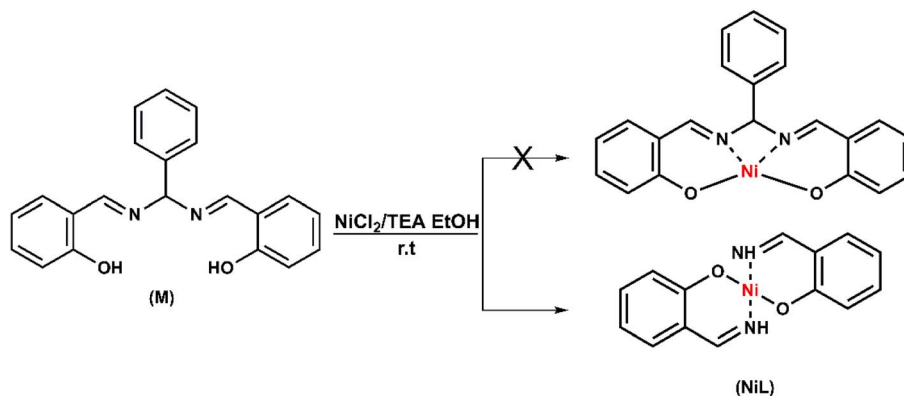
**Scheme 1** Synthesis of complex **NiL**.

decomposition of the salen ligand to imine compound during the reaction with Ni$^{II}$ ion (Fig. S1b†). The formation of this imine complex was indicated more clearly on the basis of infrared spectrum analysis. The appearance of the vibration at 3303 cm$^{-1}$ characterized the stretching vibration of the –NH group. The vibration of the C=NH imine group was indicated at 1614 cm$^{-1}$ having no difference in comparison to that on the ligand (1615 cm$^{-1}$) (Fig. S2†). The full Raman spectra of the ligand and the (**NiL**) complex showed several similarities. Especially, two bands found at 448 cm$^{-1}$ and 482 cm$^{-1}$ were attributed to the Ni–O stretching vibration (Fig. S3†). This evidence reinforced the formation of the Ni–O bond in the complex structure.

**NiL** complex was also investigated by the molecular absorption spectroscopy (Fig. 1). The π to π* intra-ligand transitions of the aromatic system and the imine group – CH=N in the complex were observed at 266 nm and 323 nm, respectively.[27] There was a shoulder at 337 nm with a molar absorptivity of 9028 L mol$^{-1}$ cm$^{-1}$, which was assigned to the charge–transfer transition in the nickel(II) Schiff-base complex.[27] In the NiCl$_2$ precursor spectrum, the $d$–$d$ transition of nickel could be observed at 408 nm with a low molar absorptivity of 14 L mol$^{-1}$ cm$^{-1}$. However, this $d$–$d$ transition changed to metal-to-ligand charge transfer in the **NiL** complex as a significantly greater molar absorptivity (5245 L mol$^{-1}$ cm$^{-1}$)

was determined (Fig. 1, zone 2).[27] In our previous study, we indicated that when the imine groups participated in the complexation with cobalt ions, the absorption peak of the ligand at 321 nm (π to π* transition of imine groups) experienced a red-shift to a higher wavelength (*e.g.* 378 and 400 nm).[26] However, in the case of the nickel complex, when compared with previous nickel Schiff-base complexes, this transition still remained at the same wavelength.[27]

The eventual chemical decomposition of the **NiL** complex was investigated in the presence of two acidic environments: acetic acid AA (p$K_a$ of 13.5 in DMF) and trifluoroacetic acid TFA (p$K_a$ of 6.0 in DMF) (Fig. 2). In the case of a weaker acid, the absorption peak was intact when increasing the amount of acid up to 70 equivalent moles suggesting that the complex was stable in this acidic environment (Fig. 2a and b).

In the shape contrast, when the TFA proton source was added, the complex solution gradually lost its colour (Fig. 2c and S4a†). When 1 or 2 molars equivalent of TFA was added, the **NiL** compound could be protonated, but this protonation did not decompose the complex. Indeed, unchanged UV-vis spectra were recorded (Fig. 2d). However, adding up to 4 equivalent molars of TFA caused the complete degradation of the **NiL**
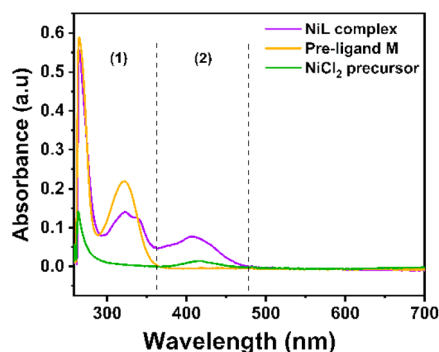


**Fig. 1** UV-vis spectra recorded for **NiL** complex, Ni-precursor and the free ligand dissolved in DMF solution.
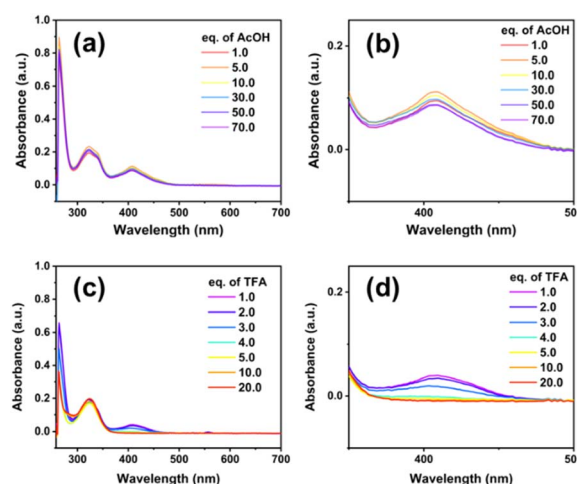


**Fig. 2** UV-vis spectra recorded for **NiL** complex dissolved in DMF in the presence of acetic acid (a and b) and trifluoroacetic acid (c and d).

complex, releasing the free ligand and nickel trifluoroacetate salt (Fig. 2d). As a result, the MLCT band completely disappeared and the absorption spectrum of the initial ligand reappeared (Fig. S4b†). Finally, the elemental analysis and ICP-MS analysis showed the similarity between the calculated and actually found elemental composition, thereby further confirming the complex structure.

### Electrochemical properties and electrocatalytic H$_2$ evolution activity

The electrochemical properties of the **NiL** complex were first investigated in an organic electrolyte, namely the DMF solvent containing 0.1 M TBATFB as the electrolyte support. Molar concentration of this compound was prepared at 1 mM. Cyclic voltammograms were recorded on a glassy carbon electrode with the potential scan rate of 50 mV s$^{-1}$ (Fig. 3).

A quasi-reversible redox event at $E_{1/2}$ of $-2.06$ V vs. Fc$^{+/0}$ with peak-to-peak separation $\Delta E$ of 62 mV was observed, which was assigned to the Ni$^{II}$/Ni$^{I}$ redox couple. In comparison to the NiCl$_2$ precursor, the NiL complex displayed the Ni$^{II}$/Ni$^{I}$ redox couple at more cathodic potential ($-2.10$ V versus $-1.73$ V vs. Fc$^{+/0}$) (Fig. S5†). This change could be explained by the fact that the electron donation of **L** ligand enriched the electron density in the Ni$^{II}$ center within the **NiL** complex, hence the reduction of **NiL** required a more cathodic potential. Additionally, there is a small reduction shoulder at $-1.96$ V vs. Fc$^{+/0}$, which was attributed to the reduction of free-imine groups within the **NiL** compound.[28–30]

We then investigated the electrocatalytic H$_2$ evolution activities of the **NiL** complex in the same DMF electrolyte solution in the presence of acetic acid (AA) as the proton source. It can be seen that with the sequent increase of AA concentration (from 0.0 to 50.0 mM), a catalytic wave emerged at a mid-wave potential $E^{\circ}_{cat}$ of $-2.05$ V vs. Fc$^{+/0}$ (Fig. 4a). This potential is close to that found for the Ni$^{II}$/Ni$^{I}$ redox couple in the absence of proton source (Fig. 3). It suggests that the reduced Ni$^{I}$ intermediate could involve in the catalysis of H$_2$ evolution. We note that this intermediate was usually found for nickel complexes such as nickel–salen;[31] nickel–thiosemicarbazone;[32] nickel–pyridylthiolate[33] or nickel–thioether.[34] It is noted that when adding 1 equivalent of acetic acid into the complex solution,



Fig. 4 Cyclic voltammograms recorded on a glassy carbon electrode for a 1 mM solution of **NiL** in DMF with the increasing amount of acetic acid added (a) and (b) shows the cyclic voltammograms recorded when adding a low concentration of acetic acid. The potential scan rate was 50 mV s$^{-1}$.

the reduction peak shifted toward the less cathodic potential (Fig. 4b). This phenomenon implies that the reduction of Ni$^{II}$ center within the **NiL** complex required lower reducing energy in the presence of a proton.

It can be explained that the protonation first occurred at the imine groups leading to the delocalization of electrons in the conjugated system, which decreased the electron density in the Ni$^{II}$ center and therefore shifted its reduction to lower reducing potential (Scheme 2). In other words, the H$_2$ evolution occurred on the **NiL** catalyst via a CE mechanism wherein C implied the chemical step and E implied the electron-transfer step. We note that the CE mechanism has been evoked for other nickel complexes, such as nickel–pyridylthiolate complex[33] or nickel–pyridino diquinoline complex[35]

To ensure that the proton reduction producing H$_2$ occurred by catalytic activities of homogeneous **NiL** complex dissolved in solution but not its eventual decomposition products, the "rinse test" being the control experiment was carried out. The glassy carbon electrode, used for recording cyclic voltammograms of a solution containing 1 mM catalyst **NiL** and 50 mM AA, was taken out and washed intensively with DMF solvent. The electrode was then immersed in a new DMF solution containing 50 mM AA without catalyst **NiL**. A negligible cathodic current was recorded. This result demonstrated the non-catalytic character of the glassy carbon electrode after being used for the catalysis assay of the **NiL** complex. In other words, no catalytically active deposit was produced from the **NiL** solution during the H$_2$ evolution catalytic assay (Fig. S6†). Hence, the catalytic H$_2$ evolution activity was solely generated by the **NiL** homogeneous catalyst but not its decomposition product. This result is quite consistent with most previous studies reporting on the stability of nickel complexes under electrochemical reduction conditions. It is noted that under the electrochemical oxidation
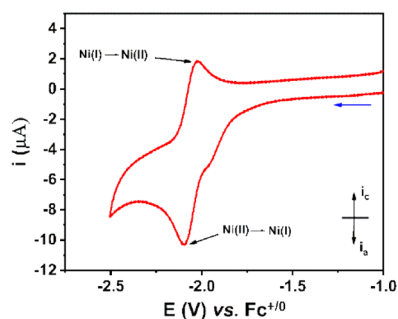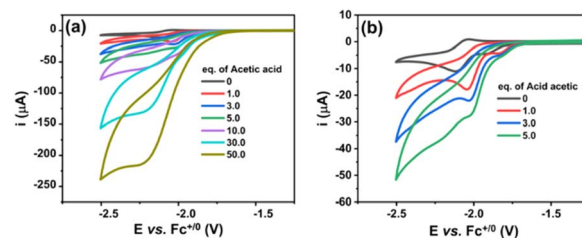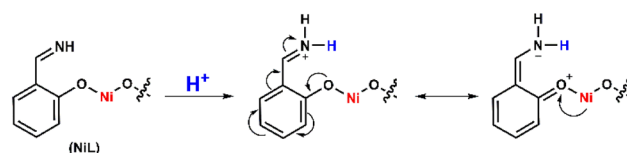


Fig. 3 Cyclic voltammograms recorded on a stationary glassy carbon electrode for the 1 mM **NiL** in DMF solution. The potential scan rate was 50 mV s$^{-1}$.



Scheme 2 Electron delocalization in the **NiL** complex induced by the protonation.

conditions, the electro-decomposition of nickel complexes such as the Ni–marcoaza complex could occur to produce $NiO_x$.[36,37]

To further evidence the stability of the **NiL** complex during the catalytic $H_2$ evolution, its solution with acetic acid added after each potential polarization, namely after recording each cyclic voltammogram, was sampled and analyzed by UV-vis absorption spectroscopy. No noticeable change was observed which clearly evidenced the remaining **NiL** structure during the $H_2$ evolution catalysis (Fig. 5).

Bulk electrolysis was then conducted at a constant potential of −2.05 V vs. $Fc^{+/0}$ using a DMF electrolyte solution containing 1 mM catalyst **NiL**, 50 mM acetic acid and 0.1 M TBATFB electrolyte support. The working electrode was a graphite electrode with a working area of 2 cm². $H_2$ gas produced was quantified employing a gas chromatography analysis. After a 3 hours electrolysis experiment, faradaic efficiency was deduced to be 49% for the catalyst **NiL**. (Fig. S7†). This result could be explained by the competitive 2-electron reduction of the free-imine moiety in the presence of a proton source. This phenomenon has been reported in previous studies when the reduction of imine functional groups was investigated and developed by using electrochemical methods.[28–30] Additionally, under longer catalysis operation time, the catalyst tended to be decomposed and deposited on the surface of the working electrode. The deposit of nickel was evidenced by the ICP-MS analysis. However, the amount of Ni metal deposited on the electrode's surface only accounted for about 9% of the total amount of **NiL** catalyst used. This decomposition could be understandable because the structure of **NiL** lacks the coordination bonds of the imine group, which were usually found in the conventional salen complexes. Such a lack of coordination bond caused the degradation of the **NiL** catalyst when it was operated under harsh conditions.

To appreciate an $H_2$-evolution catalyst and compare its performance with other catalysts, the overpotential ($\eta$) is a key parameter, which is defined as the difference between the equilibrium potential (or thermodynamic potential) of the HA/$H_2$ couple and the catalytic potential required to generate a specific catalytic current. In the case of molecular catalysts, the catalytic potential is usually determined from the half-catalytic-wave potential, and therefore defined as $E_{cat/2}$.[38]

Herein, the overpotential required for $H_2$ evolution when using **NiL** catalysts in DMF solution was determined at the half-way potential in the presence of 50 mM of acetic acid. Under such a working condition, the thermodynamic reduction potential of the acetic acid in DMF $E°(HA;H_2)$ can be estimated by the equation proposed by Artero and colleagues,[39] presenting the $E°(HA; H_2)$ value of −1.46 V vs. $Fc^{+/0}$ (see ESI†). Thus, the overpotential required for the $H_2$ evolution using **NiL** catalyst was 590 mV (Fig. S8†). In comparison with the nickel–salen-modified complex containing 3-carbon linkage, which was reported by Liu et al.,[21] the current **NiL** complex required a higher overpotential (of around 190 mV) when employing the same acetic acid as the proton source. However, we note that these two complexes were investigated in two different solvents, namely the acetonitrile for nickel–salen-modified complex and the DMF for **NiL** complex. Compared with other nickel Schiff-base complexes (without the 2-carbon linkage in the structure),[40] the current **NiL** complex showed similar catalytic activity when the difference between the two overpotential values was just 30 mV (560 mV vs. 590 mV) in the presence of acetic acid.

### Kinetic analysis and determination of rate constant

We then studied the kinetics of $H_2$ evolution using the **NiL** catalyst. Firstly, the order of catalyst concentration was examined by varying the catalyst concentration from 1.0 to 3.0 mM while using the same solution of 70 mM acetic acid. The catalytic rates were recorded by cyclic voltammetry, with potential scan rates varying from 50 mV s⁻¹ to 1000 mV s⁻¹.

In this case, the concentration of acetic acid was largely in excess to ensure that there was no substrate depletion at the electrode when the catalytic operation was carried out. Fig. 6a shows the evolution of maximum catalytic current at different potential scan rates as a function of the catalyst concentration. From the observation of linear dependence could deduce the first order of the **NiL** catalyst. Besides that, the ratio of the catalytic current to the peak current displayed the same linear dependence on the acid concentration up to 150 mM, indicating a second-order dependence of the catalytic rate on the acid substrate (Fig. 6b).[31,41] The performance of catalyst could be greatly influenced by the diffusion rate to the electrode surface at a given potential scan rate. By using the Randle–Sevcik equation, the cathodic peak current was plotted against the
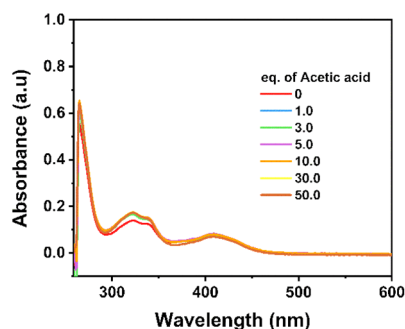


**Fig. 5** UV-vis spectra recorded for the solution containing **NiL** complex and acetic acid after being conditioned under the catalytic $H_2$ evolution conditions.



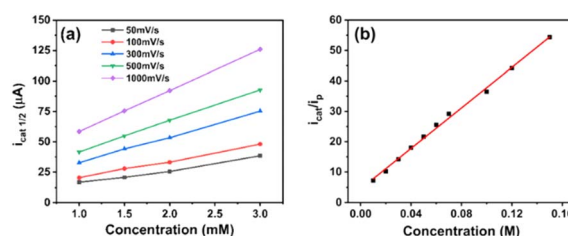**Fig. 6** Plot of $i_{cat1/2}$ (half-way catalytic current) in the function of the concentration of **NiL** complex at different potential scan rates in the presence of 7 0 mM acetic acid as the proton source (a). A plot of $i_{cat}/i_p$ as a function of acetic acid concentration while using 1 mM **NiL**, the potential scan rate of 50 mV s⁻¹ (b).

square root of the scan rates. From the slope of the linear plotting, the diffusion coefficient ($D$) value of the **NiL** complex was deduced to be $1.14 \times 10^{-5}$ cm$^2$ s$^{-1}$ (see ESI Fig. S9†).

To determine the kinetic parameters, the mechanistic pathway for HER needs to be proposed first. As aforementioned in the potential polarization curve analysis, the first step of H$_2$ evolution catalysis was assigned for the protonation of **NiL** complex (denoted hereafter as C for the chemical step) and this intermediate underwent one-electron reduction to obtain the Ni$^I$ species (denoted hereafter as $E$ for the electron-transfer step).

This Ni$^I$ complex experienced the second CE process resulting in the evolution of the H$_2$ molecule.[42–46] In other words, the H$_2$ evolution occurred on the **NiL** catalyst *via* a CECE mechanism (Scheme 3). Although the CECE mechanism is not as popular as the ECEC one, CECE was evoked for some nickel molecular catalysts.[31,33,35] Based on the above catalytic pathway, there are two approaches commonly used for the estimation of catalytic rate constant and maximal turnover frequency (TOF$_{max}$), foot-of-the-wave analysis (FOWA) and plateau current analysis (PCA). Despite benefits when investigating electrocatalysts under the non-pure kinetic condition[47] (or S-shaped catalytic wave), Grapperhaus indicated that FOWA was not suitable for the complexes involving the initial protonation step in the HER mechanism (CECE or CCEE).[41] PCA was suggested as an alternative method when studying the kinetics of the catalytic operation. One drawback of this calculation is the absence of a perfect S-shaped catalytic wave, however, it is still useful for the preliminary assignment of the catalytic performance.

For such a CECE mechanism, the relationship between the rate constant and the ratio of the catalytic current over the peak current is described by eqn (1) (ref. 41) wherein $i_{cat}$ is the catalytic current (mA), $i_p$ is the cathodic peak current (mA), $R = 8.314$ J mol$^{-1}$ K, $T = 299$ K, $F = 96\ 485$ C mol$^{-1}$, $\nu$ is scan rate (V s$^{-1}$), and $k_{obs} = k_{cat}[H^+]^2$ (s$^{-1}$).

$$\frac{i_{cat}}{i_p} = \frac{n}{0.4463} \times \sqrt{\frac{RTk_{obs}}{F\nu}} \tag{1}$$

To decrease the restriction of substrate consumption (acetic acid), we expanded the quantity of the acid concentration to 150 mM to ensure that $i_{cat}$ was not limited by substrate diffusion. It means that the catalytic wave could achieve zone KD.[47,48] The calculation of $k_{obs}$ values and corresponding $k_{cat}$ values are shown in Table S1.† The changing trend of catalytic rate constants can be observed clearly in Fig. 7.
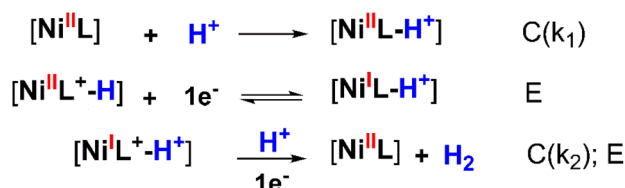


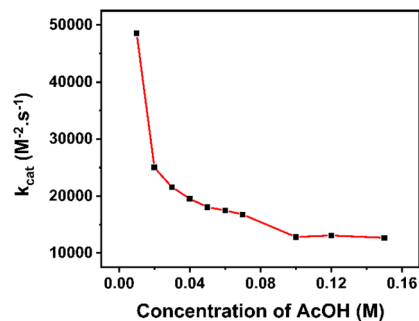**Fig. 7** $k_{cat}$ extracted from PCA in various concentrations of acetic acid.

At lower concentrations of the H$^+$ substrate, there is a competition between the consumption of the H$^+$ substrate by the rate-determining step and the diffusion of new H$^+$ substrate to the electrode. The depletion of the acid led to a high rate of catalysis. With the concentration of acetic acid over 100 mM, the rate constant values attained the plateau, implying that the catalyst operates under the condition of no substrate consumption (reached zone KD). In other words, the catalyst has gradually approached the "pure kinetic" zone, so the reaction rate has slowed down and reached an average catalytic rate constant of about 12 860 M$^{2-}$ s$^{-1}$. Therefore, the TOF$_{max}$ value approximates $k_{cat}[AA]^2$ and could be extrapolated to be 12 860 s$^{-1}$ for 1 M acetic acid concentration.

## Conclusions

To conclude, an unusual imine-type nickel complex (**NiL**) was prepared. The product was generated by the complexation of nickel salt with the *in situ* formed **L** ligand (**L** is 2-(iminomethyl) phenol). The structure of the **NiL** complex was determined by physical methods (NMR; IR; Raman; UV-vis and elemental analysis). In a DMF electrolyte solution, using this **NiL** complex as an electrocatalyst and in the presence acetic acid as a proton source, the catalytic H$_2$ evolution emerged at potential close to that of Ni$^{II}$/Ni$^I$ reduction. Bulk electrolysis at $-2.05$ V *vs.* Fc$^{+/0}$ produced H$_2$ gas with a faradaic yield of 49%. Non-unity faradaic yield was due to the competition between the catalytic H$^+$ reduction generating H$_2$ and the 2-electron reduction of the free-imine group in the **L** ligand. Based on the proposed CECE mechanism for the H$_2$ evolution, theoretical PCA analysis allowed quantifying the rate constants and maximal turnover frequency of **NiL** catalyst; with 1 M acetic acid, TOF$_{max}$ was estimated to be about 12 860 s$^{-1}$.

## Data availability

The data supporting this article have been included as part of the ESI.†

## Author contributions

All authors have given approval to the final version of the manuscript.



**Scheme 3** CECE mechanism proposed for the H$_2$ evolution on **NiL** catalyst (wherein [Ni$^I$] and [Ni$^{II}$] represented the active sites).

## Conflicts of interest

There are no conflicts to declare.

## Acknowledgements

## References

1 J. O. Abe, A. P. I. Popoola, E. Ajenifuja and O. M. Popoola, *Int. J. Hydrogen Energy*, 2019, **44**, 15072–15086.

2 A. I. Osman, N. Mehta, A. M. Elgarahy, M. Hefny, A. Al-Hinai, A. a. H. Al-Muhtaseb and D. W. Rooney, *Environ. Chem. Lett.*, 2022, **20**, 153–188.

3 T. T. Le, P. Sharma, B. J. Bora, V. D. Tran, T. H. Truong, H. C. Le and P. Q. P. Nguyen, *Int. J. Hydrogen Energy*, 2024, **54**, 791–816.

4 S. Wang, A. Lu and C.-J. Zhong, *Nano Convergence*, 2021, **8**, 4.

5 M. Wang, L. Chen and L. Sun, *Energy Environ. Sci.*, 2012, **5**, 6763–6778.

6 V. S. Thoi, Y. Sun, J. R. Long and C. J. Chang, *Chem. Soc. Rev.*, 2013, **42**, 2388–2400.

7 J. R. McKone, S. C. Marinescu, B. S. Brunschwig, J. R. Winkler and H. B. Gray, *Chem. Sci.*, 2014, **5**, 865–878.

8 I. Roger, M. A. Shipman and M. D. Symes, *Nat. Rev. Chem*, 2017, **1**, 0003.

9 J. Mohammed-Ibrahim and X. Sun, *J. Energy Chem.*, 2019, **34**, 111–160.

10 D. Zhang, J. Z. Soo, H. H. Tan, C. Jagadish, K. Catchpole and S. K. Karuturi, *Adv. Energy Sustainability Res.*, 2021, **2**, 2000071.

11 J. D. McCool, S. Zhang, I. Cheng and X. Zhao, *Chin. J. Catal.*, 2022, **43**, 3019–3045.

12 W. Lubitz, H. Ogata, O. Rüdiger and E. Reijerse, *Chem. Rev.*, 2014, **114**, 4081–4148.

13 N. A. Eberhardt and H. Guan, *Chem. Rev.*, 2016, **116**, 8373–8426.

14 S. J. C. Robinson and D. M. Heinekey, *Chem. Commun.*, 2017, **53**, 669–676.

15 G.-G. Luo, H.-L. Zhang, Y.-W. Tao, Q.-Y. Wu, D. Tian and Q. Zhang, *Inorg. Chem. Front.*, 2019, **6**, 343–354.

16 L. Tong, L. Duan, A. Zhou and R. P. Thummel, *Coord. Chem. Rev.*, 2020, **402**, 213079.

17 J.-W. Wang, W.-J. Liu, D.-C. Zhong and T.-B. Lu, *Coord. Chem. Rev.*, 2019, **378**, 237–261.

18 L. Chen, G. Chen, C.-F. Leung, S.-M. Yiu, C.-C. Ko, E. Anxolabéhère-Mallart, M. Robert and T.-C. Lau, *ACS Catal.*, 2015, **5**, 356–364.

19 Y.-X. Zhang, L.-Z. Tang, Y.-F. Deng and S.-Z. Zhan, *Inorg. Chem. Commun.*, 2016, **72**, 100–104.

20 H. Shao, S. K. Muduli, P. D. Tran and H. S. Soo, *Chem. Commun.*, 2016, **52**, 2948–2951.

21 X.-S. Hong, D. Huo, W.-J. Jiang, W.-J. Long, J.-D. Leng, L. Tong and Z.-Q. Liu, *ChemElectroChem*, 2020, **7**, 4956–4962.

22 C.-L. Wang, H. Yang, J. Du and S.-Z. Zhan, *Int. J. Hydrogen Energy*, 2021, **46**, 32480–32489.

23 A. Barma, A. Sarkar, S. Roy, B. Show and P. Roy, *ChemistrySelect*, 2023, **8**, e202302725.

24 H. Jadamus, Q. Fernando and H. Freiser, *J. Am. Chem. Soc.*, 1964, **86**, 3056–3059.

25 G. Mukherjee, S. N. Poddar and K. Dey, *Transition Met. Chem.*, 1987, **12**, 323–327.

26 T. H. To, D. B. Tran, V. Thi Thu Ha and P. D. Tran, *RSC Adv.*, 2022, **12**, 26428–26434.

27 D. Tomczyk, L. Nowak, W. Bukowski, K. Bester, P. Urbaniak, G. Andrijewski and B. Olejniczak, *Electrochim. Acta*, 2014, **121**, 64–77.

28 A. J. Fry and R. G. Reed, *J. Am. Chem. Soc.*, 1969, **91**, 6448–6451.

29 D. K. Root and W. H. Smith, *J. Electrochem. Soc.*, 1982, **129**, 1231.

30 A. Wang, X. Liu, W. Gao, L. Ma, S. Liu, G. Zhang, M. Zhou, X. Jia and J. Chen, *Chem. Commun.*, 2022, **58**, 9906–9909.

31 C.-B. Li, Y. Chu, J. He, J. Xie, J. Liu, N. Wang and J. Tang, *ChemCatChem*, 2019, **11**, 6324–6331.

32 T. Straistari, J. Fize, S. Shova, M. Réglier, V. Artero and M. Orio, *ChemCatChem*, 2017, **9**, 2262–2268.

33 Z. Han, L. Shen, W. W. Brennessel, P. L. Holland and R. Eisenberg, *J. Am. Chem. Soc.*, 2013, **135**, 14659–14669.

34 D. Hong, Y. Tsukakoshi, H. Kotani, T. Ishizuka, K. Ohkubo, Y. Shiota, K. Yoshizawa, S. Fukuzumi and T. Kojima, *Inorg. Chem.*, 2018, **57**, 7180–7190.

35 K. Majee, J. Patel, S. Rai, B. Das, B. Panda and S. K. Padhi, *Phys. Chem. Chem. Phys.*, 2016, **18**, 21640–21650.

36 J. Singh, G. Hundal and R. Gupta, *Eur. J. Inorg. Chem.*, 2008, **2008**, 2052–2063.

37 J. Hessels, F. Yu, R. J. Detz and J. N. H. Reek, *ChemSusChem*, 2020, **13**, 5625–5631.

38 A. M. Appel and M. L. Helm, *ACS Catal.*, 2014, **4**, 630–633.

39 V. Fourmond, P.-A. Jacques, M. Fontecave and V. Artero, *Inorg. Chem.*, 2010, **49**, 10338–10347.

40 A. Barma, M. Chakraborty, S. K. Bhattacharya, P. Ghosh and P. Roy, *Mater. Adv.*, 2022, **3**, 7655–7666.

41 A. Z. Haddad, S. P. Cronin, M. S. Mashuta, R. M. Buchanan and C. A. Grapperhaus, *Inorg. Chem.*, 2017, **56**, 11254–11265.

42 T. L. James, L. Cai, M. C. Muetterties and R. H. Holm, *Inorg. Chem.*, 1996, **35**, 4148–4161.

43 O. R. Luca, J. D. Blakemore, S. J. Konezny, J. M. Praetorius, T. J. Schmeier, G. B. Hunsinger, V. S. Batista, G. W. Brudvig, N. Hazari and R. H. Crabtree, *Inorg. Chem.*, 2012, **51**, 8704–8709.

44 Y. Han, H. Fang, H. Jing, H. Sun, H. Lei, W. Lai and R. Cao, *Angew. Chem., Int. Ed.*, 2016, **55**, 5457–5462.

45 R. Jain, A. A. Mamun, R. M. Buchanan, P. M. Kozlowski and C. A. Grapperhaus, *Inorg. Chem.*, 2018, **57**, 13486–13493.

46 S. Chakrabarti, S. Sinha, G. N. Tran, H. Na and L. M. Mirica, *Nat. Commun.*, 2023, **14**, 905.

47 K. J. Lee, N. Elgrishi, B. Kandemir and J. L. Dempsey, *Nat. Rev. Chem*, 2017, **1**, 0039.

48 E. S. Rountree, B. D. McCarthy, T. T. Eisenhart and J. L. Dempsey, *Inorg. Chem.*, 2014, **53**, 9983–10002.